Single Pixel Performance of a 32 x 32 Ti/Au TES Array With Broadband X-Ray Spectra

D'andrea, Matteo; Taralli, Emanuele; Akamatsu, Hiroki; Gottardi, Luciano; Nagayoshi, Kenichiro; Ravensberg, Kevin; Ridder, Marcel L.; Vaccaro, Davide; De Vries, Cor P.; De Wit, Martin

Important note
To cite this publication, please use the final published version (if applicable).
Please check the document version above.

Single Pixel Performance of a 32 × 32 Ti/Au TES Array With Broadband X-Ray Spectra

Matteo D'Andrea , Emanuele Taralli, Hiroki Akamatsu, Luciano Gottardi , Kenichiro Nagayoshi,
Kevin Ravensberg, Marcel L. Ridder, Davide Vaccaro, Cor P. de Vries, Martin de Wit , Marcel P. Bruijn,
Ruud W. M. Hoogeveen, and Jian-Rong Gao

Abstract—**We are developing a kilo-pixels Ti/Au TES array as a backup option for Athena X-IFU. Here we report on single-pixel performance of a 32 × 32 array operated in a Frequency Division Multiplexing (FDM) readout system, with bias frequencies in the range 1–5 MHz. We have tested the pixels response at several photon energies, by means of a ^{55}Fe radioactive source (emitting Mn-Kα at 5.9 keV) and a Modulated X-ray Source (MXS), providing Cr-Kα at 5.4 keV and Cu-Kα at 8.0 keV). First, we report the procedure used to perform the detector energy scale calibration, usually achieving a calibration accuracy better than ~0.5 eV in the 5.4–8.9 keV energy range. Then, we present the measured energy resolution at the different energies (best single pixel performance: $\Delta E_{\mathrm{FWHM}} = 2.40 \pm 0.09$ eV @ 5.4 keV; 2.53 $\pm$ 0.10 eV @ 5.9 keV; 2.78 $\pm$ 0.16 eV @ 8.0 keV), investigating also the performance dependency from the pixel bias frequency and the count rate. Thanks to long background measurements (~1 d), we finally detected also the Al-Kα line at 1.5 keV, generated by fluorescence inside the experimental setup. We analyzed this line to obtain a first assessment of the single-pixel performance also at low energy ($\Delta E_{\mathrm{FWHM}} = 1.91$ eV $\pm$ 0.21 eV @ 1.5 keV), and to evaluate the linearity of the detector response in a large energy band (1.5–8.9 keV).**

Index Terms—**Energy calibration, energy resolution, MXS, TES, X-IFU, x-ray detectors.**

I. INTRODUCTION

A THENA is a large X-ray observatory (0.2–12 keV energy band), planned to be launched by ESA in the early 2030 s.

Matteo D'Andrea was with the NWO-I/SRON Utrecht, Utrecht 3584 CA, The Netherlands. He is now with INAF/IAPS Roma, 00133 Rome, Italy (e-mail: matteo.dandrea@inaf.it).

Emanuele Taralli, Hiroki Akamatsu, Luciano Gottardi, Kenichiro Nagayoshi, Kevin Ravensberg, Marcel L. Ridder, Davide Vaccaro, Cor P. de Vries, Martin de Wit, Marcel P. Bruijn, and Ruud W. M. Hoogeveen are with the NWO-I/SRON Utrecht, Utrecht 3584 CA, The Netherlands (e-mail: e.taralli@sron.nl; H.akamatsu@sron.nl; l.gottardi@sron.nl; k.nagayoshi@sron.nl; k.ravensberg@sron.nl; M.L.Ridder@sron.nl; d.vaccaro@sron.nl; c.p.de.vries @sron.nl; m.de.wit@sron.nl; M.P.Bruijn@SRON.nl; R.W.M.Hoogeveen@ sron.nl).

Jian-Rong Gao is with NWO-I/SRON Utrecht, Utrecht 3584 CA, The Netherlands and also with the Faculty of Applied Science, Delft University of Technology, Delft 2600 AA, The Netherlands (e-mail: J.R.Gao@sron.nl).

Color versions of one or more figures in this article are available at https: //doi.org/10.1109/TASC.2021.3065303.

Digital Object Identifier 10.1109/TASC.2021.3065303

One of the two focal plane instruments is the X-ray Integral Field Unit (X-IFU) [1], which is a cryogenic spectrometer able to perform simultaneously detailed imaging (5" angular resolution over a Field of View of 5 arcmin diameter) and high resolution spectroscopy ($\Delta E_{\mathrm{FWHM}} < 2.5$ eV at E < 7 keV and $\Delta E_{\mathrm{FWHM}} < 5$ eV at E $= 10$ keV). The X-IFU will address the *Hot and Energetic Universe* science theme, providing in particular: integral field spectroscopic mapping of the hot plasma in galaxy clusters; weak spectroscopic detection of absorption and emission lines from the Warm Hot Intergalactic Medium (WHIM); physical characterization of the most energetic phenomena in the Universe (e.g. AGN winds and outflows) [2]. The core of the instrument is a large array of ~3000 Mo/Au Transition Edge Sensor (TES) microcalorimeters, provided by NASA-Goddard and operated at a 50 mK thermal bath temperature [3], [4].

We are developing a Ti/Au TES array as a European backup technology for Athena X-IFU. In the recent past, the work has been focused in the optimization of the pixels design [5], [6], [7], and their characterization under both AC and DC bias [8]. Furthermore, kilo-pixel arrays have been produced and operated in a Frequency Division Multiplexing (FDM) readout system, in order to evaluate the homogeneity of the pixels characteristics and performances [9], [10], [11]. In these tests, the detector response has been usually evaluated at 5.9 keV, by using the Mn K α calibration line generated by means of a radioactive ^{55}Fe source.

In this work, we present single-pixel performance at different photon energies (i.e., 1.5 keV, 5.4 keV, 5.9 keV and 8.9 keV), and we preliminary investigate the achievable energy scale calibration accuracy, the detector linearity and the count-rate effect on the performance.

II. EXPERIMENTAL SETUP

The detector under test is a uniform 32 × 32 pixels array, with 240 × 240 μm ^{2} Au absorbers (2.35 μm thickness). The TESs have an aspect ratio (lenght × width) of 140 × 30 μm^2, and consist of Ti/Au (35 nm/ 200 nm) bilayers with a critical temperature $T_{\mathrm{C}} \sim 90$ mK and a normal resistance $R_{\mathrm{N}} \sim 120$ mΩ. The pixel heat capacity is C ~ 0.85 pJ/K at T_{C}, and the expected thermal conductance is G ~ 95 pW/K at T_{C}. More details about the detector design and fabrication can be found in [9], while a deep characterization of the array has been reported in [10] and [11].

The detector has been operated in our FDM readout system [12], [13]. Under the FDM scheme, TES are coupled to high-Q LC filters [14] and AC biased at MHz frequencies. The
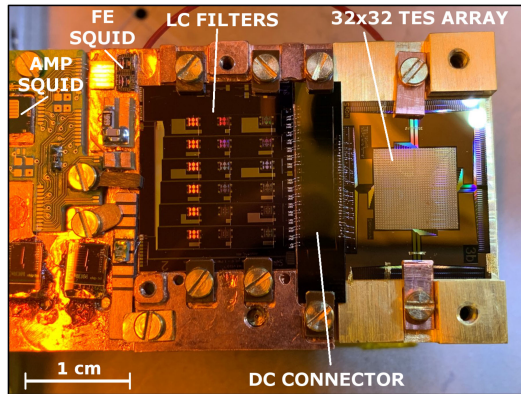
Fig. 1.   Picture of the setup (cold stage) used to operate the kilo-pixel array. The labels indicate the main components.

Fig. 2.   Energy spectrum measured by Px8 (2.7 MHz bias frequency) with the MXS turned ON (black curve) and OFF (red curve).

TES signals are then summed and amplified by a low-noise two-stage SQUID amplifier chain, and finally demodulated at room temperature by digital electronics. The main parts of the cold stage setup are shown in Fig. 1. We have used a 18 channels LC-filter chip, with a coil inductance $L = 2 \ \mu H$ and a DC connector chip. The pixels bias frequencies are between 1 and 5 MHz. The SQUID amplifiers are a VTT J3 (Front End SQUID) and a VTT F5 (Amp SQUID).

The setup has been installed in a dilution refrigerator, and thermoregulated at a temperature of 40 mK. It has been suspended with respect to the cryostat mixing chamber via kevlar strings, in order to avoid microvibrations due to the pulse tube operation, and magnetically shielded by a superconducting aluminum shield (at cold), and by a mu-metal shield (outside the cryostat).

The detector has been illuminated both by a radioactive ^{55}Fe source (from the back side) and a Modulated X-ray Source (MXS, from the front side). The MXS is a device able to produce X-rays with an adjustable count rate, by hitting target materials with accelerated electron, which are emitted by a photocathode stimulated by UV leds. Details about the MXS design are reported in [15]. The MXS has been vacuum tight connected to an aperture in the cryostat Outer Vacuum Chamber. All the thermal shields inside the cryostat have been provided with apertures covered with 20 microns thick mylar coated with 200 nm Al. The main purpose of such mylar windows is to block the stray light and let the X-ray pass through the cryostat.

Fig. 2 shows the comparison of the energy spectra acquired by one of the detector pixels (Px8, 2.7 MHz bias frequency) with the MXS turned ON and OFF. The Mn-Kα (5.9 keV) and Mn-Kβ (6.4 keV) lines are emitted by the ^{55}Fe source. The MXS provides the Cr-Kα (5.4 keV), Cr-Kβ (5.9 keV), Cuk-Kα (8.0 keV) and Cu-Kβ (8.9 keV) lines, and the bremsstrahlung continuum. In addition, two low-energy lines are slightly visible in the spectra, generated by fluorescence inside the setup: the Al-Kα at 1.5 keV (generated in the aluminum foils used to attenuate the ^{55}Fe source), and the Si-Kα at 1.7 keV (generated in the detector substrate).

III. ANALYSIS PROCEDURE & ENERGY SCALE CALIBRATION

We have operated the TES array in single-pixel mode configuration, biasing one pixel at a time, while all the others are left
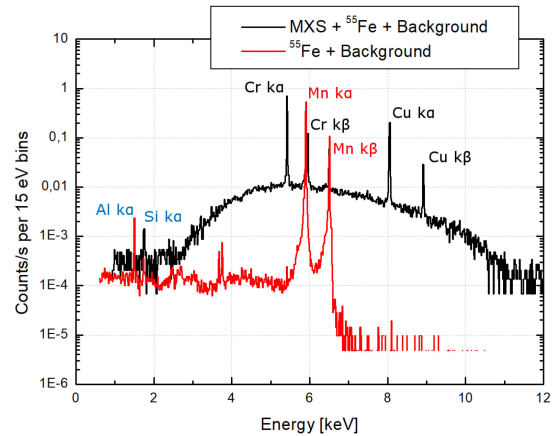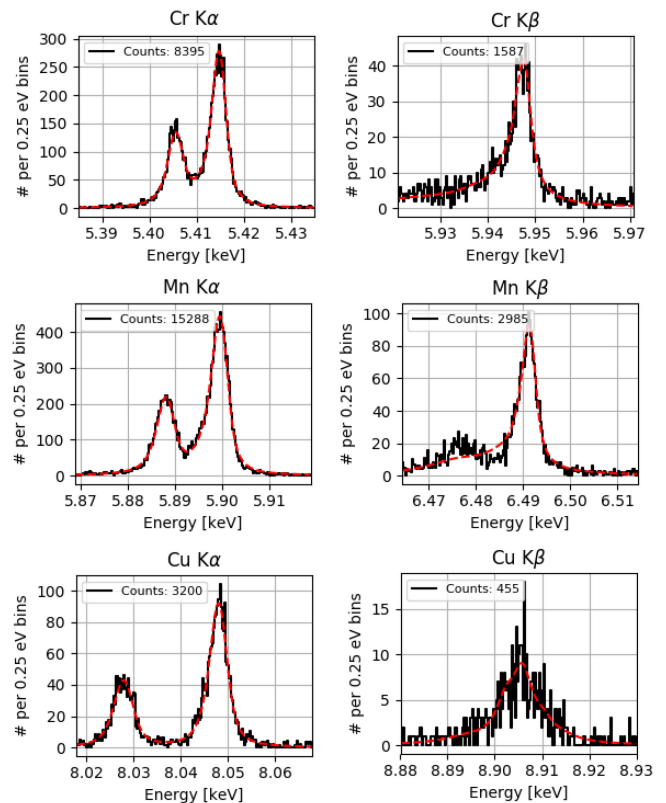

Fig. 3.   Preliminary fit of the main Kα and Kβ lines (generated by MXS and internal ^{55}Fe X-ray source) acquired by Px1 biased at 1.1 MHz.

Fig. 4.   (Left) Measured energy shift of the detected lines as a function of the energy, as obtained by the preliminary fit (data from Px1 biased at 1.1 MHz). The blue dashed lines is a 3th order polynomial fit of the data. (Right) Residuals of the 3th order polynomial fit. The fit accuracy is better than 0.5 eV.

Fig. 5. Best fit to data (red lines) for each detected Kα line (MXS and internal 55Fe X-ray source) for Px1 biased at @ 1.1 MHz. The lines intrinsic shape (blue lines) has been described according to [16].

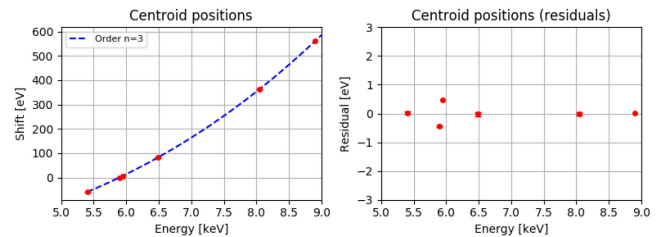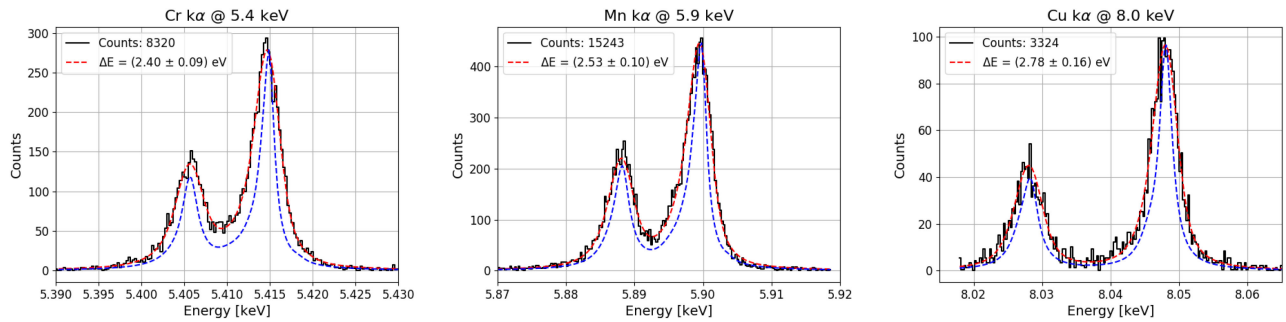in the superconducting state. We have configured the MXS in order to have a count-rate of ∼3 counts per second per pixel, and collected 50 000 pulses per measure. To analyze the data, we have then proceeded as follows:

1) We have generated pulse and noise templates, and performed the pulses optimal filtering. The pulse template has been generated by averaging 100 pulses in the 5.9 keV line;

2) We have linearly calibrated the energy scale by roughly using the most prominent line in the spectrum (i.e., the Mn-Kα at 5.9 keV);

3) We have preliminarily fitted all the main Kα and Kβ lines in the spectrum (Fig. 3). The intrinsic line shapes have been described according to the ASTRO-H SXS Calibration Database for Line Fit [16];

4) From the preliminary fits, we obtained the energy shift of each line with respect to its real position. We have then fitted the measured shifts as a function of the energy with a 3th order polynomial (Fig. 5 - Left), and used the obtained Shift (E) function to correct the energy scale calibration. Note that the fit residuals (Fig. 5 - Right) represent the final energy calibration accuracy. With this method, we have usually achieved an accuracy better than ∼0.5 eV in the energy range between 5.4 and 8.9 keV (for comparison, the X-IFU will require a Mean Knowledge Error of the energy scale smaller than 0.4 eV in the 0.2 to 7 keV range [17]);

5) We have finally re-fitted the Kα lines in the spectrum to assess the detector energy resolution at the different energies. Before this final fit procedure, we performed a simple bremsstrahlung subtraction from the lines (∼1 count per bin subtracted).

IV. Energy Resolution

The best measured energy resolutions at the different energies are shown in Fig. 4. The spectra have been acquired using the Px1 (1.1 MHz bias frequency) in single-pixel readout, and they show $\Delta E_{FWHM} = (2.40 \pm 0.09)$ eV @ 5.4 keV; (2.53 ± 0.10) eV @ 5.9 keV and (2.78 ± 0.16) eV @ 8.0 keV. The performance achieved at 5.9 keV is consistent with the one previously reported for this array [10], validating both the data analysis procedure and the new experimental setup with the MXS.

We have characterized several pixels during this measurement run, obtaining consistent results. Fig. 6 shows the energy resolution measured for Cr-Kα, Mn-Kα and Cu-Kα comparing 3 pixels at different bias frequencies: Px1 at 1.1 MHz, Px8 at 2.7 MHz and Px16 at 4.6 MHz (i.e., low, mid and high
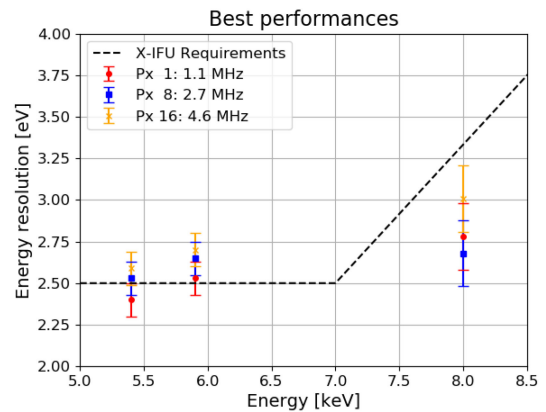

Fig. 6. Energy resolution as a function of the MXS emission line energies for 3 pixels at different bias frequencies: Px1 at 1.1 MHz, Px8 at 2.7 MHz and Px16 at 4.6 MHz. The dashed black line represents the X-IFU requirement at instrument level.

bias frequency). All the measurements have been performed in single-pixel readout. The dashed black line represents the final X-IFU requirement at instrument level, and it is overplotted just for reference. Note that, for each pixel, the energy resolution degradation between 5.9 and 8.0 keV (< 0.3 eV) is lower than the one requested by the X-IFU requirements (∼ 0.8 eV).

V. Low-Energy Response & Linearity

To investigate the detector behavior also at low energy, we performed long measurements (∼1 day of observing time) to detect the background Al and Si fluorescence lines generated inside the setup (slightly visible in the spectra in Fig. 2). This allowed us to estimate the energy resolution at 1.5 keV, and to perform a first assessment of the detector linearity in a large energy band.

Fig. 7 shows the Al-Kα complex acquired in a 20 h acquisition with Px 8 (2.7 MHz bias frequency). The measured energy resolution is $\Delta E_{FWHM} = (1.91 \pm 0.21)$ eV @ 1.5 keV. In this case, the proper energy scale calibration has been obtained by linearly fitting the centroid position of the Al-Kα (1.49 keV) and the Si-Kα (1.74 keV) lines. Because of the low Si-Kα count rate (∼80 counts in 20 hours), it has been not possible to assess the detector performance also at that energy.

Considering the whole energy range we have explored so far (from 1.5 to 8.9 keV), we can estimate the linearity of the detector. Fig. 8 shows the optimal filtering output parameter (i.e.,
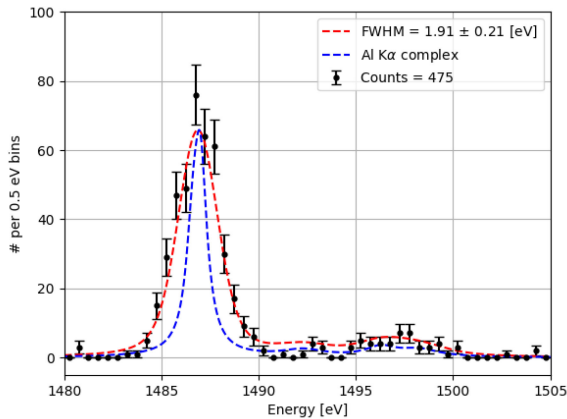
Fig. 7. Best fit (red line) of the detected Al Kα line for Px8 biased at @ 2.7 MHz. The line intrinsic shape (blue line) has been described according to [16].

Fig. 9. Energy resolution of the Cr-Kα line (5.4 keV) as a function of the count rate. Red points are average values over the three pixels biased at 1.1, 2.7 and 4.6 MHz. The blue points indicate the fraction of good events used to fit the spectra. Consider that on the X-IFU 30 cps/pixel roughly correspond to 1 Crab flux.

average flux of the supernova remnant CasA ($\sim$2.1 cps/pixel) with undegraded energy resolution and >80% high resolution events [17].

Note that here, in single-pixel readout, the primary mechanism of resolution degradation is the induced thermal instability on the pixel baseline. To proper evaluate the effect of the thermal crosstalk due to the neighbor pixels, we have performed also a dedicated measurements in multiplexed readout. This activity is reported in another paper in this issue [11].
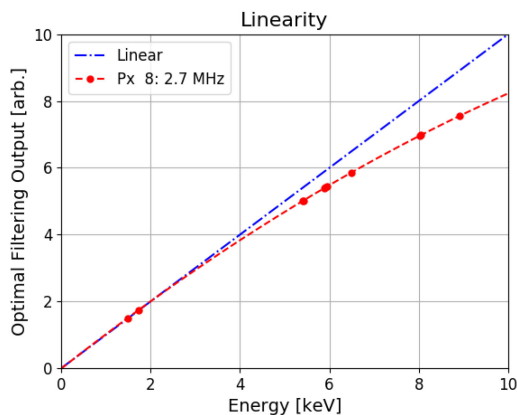

Fig. 8. Detector linearity in the range from 1.5 to 9 keV. The optimal filtering output is shown as a function of the detected line energies (red points). The dashed blue line is the linear trend calibrated on the low energy lines.

the normalized area of the optimal filtered pulses, which we use as optimal energy estimator) obtained for each detected emission lines as a function of the real lines energy. The dashed blue line is the linear trend calibrated on the detected low energy lines. We observe a deviation from the linearity of 8% at 5.9 keV and 15% at 8.9 keV.

VI. COUNT RATE EFFECT

Finally, we have performed a preliminary investigation of the energy resolution trend as a function of the count rate on the pixels. The emission rate of the MXS can be indeed increased by increasing the current in the UV-LEDs. Fig. 9 shows the measured energy resolution of the Cr-Kα line (5.4 keV) as a function of the count rate. The red points are averaged values over the three pixels biased at 1.1, 2.7 and 4.6 MHz, and operated in single-pixel readout. The blue line represent the fraction of good events used to fit the spectra. We performed a very simple pulse selection, in which we reject events where multiple pulses are detected within our optimal record lenght (26 ms). We observe that for up to around 10 counts per second no significant performance degradation is visible, and that the fraction of high resolution events is higher than 80%. Just for reference, consider that one of the X-IFU requirements is to observe the
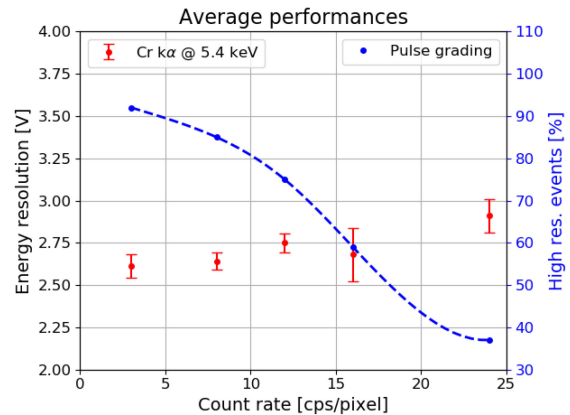
VII. CONCLUSION

We are developing a large Ti/Au TES array as a backup technology for ATHENA X-IFU. In this work, we have presented the single-pixel performance at different X-ray energies of a uniform 32×32 pixels prototype, which has been operated in the FDM readout system. The achieved energy scale calibration accuracy is usually better than $\sim$0.5 eV in the range 5.4–8.9 keV. We have measured as best single pixel performance: $\Delta E_{\mathrm{FWHM}} = (1.91 \pm 0.21)$ eV @ 1.5 keV, (2.40 ± 0.09) eV @ 5.4 keV, (2.53 ± 0.10) eV @ 5.9 keV, (2.78 ± 0.16) eV @ 8.0 keV. Finally, we have not noticed performance degradation as a function of the count rate, up to $\sim$10 count/s.

These results represent a promising first reference for the kilopixel array behavior in a large energy band, as well as conclude an extensive array characterization including performance and characteristics uniformity [10] and thermal crosstalk minimization [11]. A further optimization of the pixel design, already showing significant performance improvement [7], could lead in the near future to demonstrate a full array inside the X-IFU requirements.

REFERENCES

[1] F. Pajot *et al.*, "The athena x-ray integral field unit (X-IFU)," *J. Low Temp Phys.*, vol. 193, pp. 901–907, 2018.

[2] D. Barret and the Science Advisory Team, 2019, "Science with the athena x-ray integral field unit, X-IFU preliminary requirements review," Accessed: Mar. 22, 2021. [Online]. Available: http://x-ifu.irap.omp. eu/wp-content/uploads/2019/01/XIFU-SN-XI-09012019-IRAP.pdf, Visited 27/11/2020

[3] A. R. Miniussi *et al.*, "Performance of an x-ray microcalorimeter with a 240 μm absorber and a 50 μm TES bilayer," *J. Low Temp Phys.*, vol. 193, pp. 337–343, 2018.

[4] M. Durkin *et al.*, "Demonstration of athena X-IFU compatible 40-Row time-division-multiplexed readout," *IEEE Trans. Appl. Supercond.*, vol. 29, no. 5, Aug. 2019, Art. no. 2101005.

[5] P. Khosropanah *et al.*, "Development of TiAu TES x-ray calorimeters for the X-IFU on ATHENA space observatory," *Proc. SPIE 10699, Space Telescopes and Instrum. 2018: Ultraviolet Gamma Ray*, vol. 10699, Jul. 2018, Art. no. 106991M

[6] E. Taralli *et al.*, "Characterization of high aspect-ratio TiAu TES x-ray microcalorimeter array under AC bias," *J. Low Temp Phys.*, vol. 199, pp. 80–87, 2020.

[7] M. de Wit *et al.*, "High aspect ratio transition edge sensors for x-ray spectrometry," *J. Appl. Phys.*, vol. 128, 2020, Art. no. 224501

[8] E. Taralli *et al.*, "AC/DC characterization of a Ti/Au TES with Au/Bi absorber for x-ray detection," *J. Low Temp Phys.*, vol. 199, pp. 102–109, 2020.

[9] K. Nagayoshi *et al.*, "Development of a Ti/Au TES microcalorimeter array as a backup sensor for the Athena/X-IFU instrument," *J. Low Temp Phys.*, vol. 199, pp. 943–948, 2020.

[10] E. Taralli *et al.*, "Performance and uniformity of a kilo-pixel array of Ti/Au transition-edge sensor microcalorimeters," *Rev. Sci. Instrum.*, vol. 92, 2021, Art. no. 023101.

[11] E. Taralli *et al.*, "TiAu TES 32x32 pixel array: Uniformity, thermal cross-talk and performance at different X-ray energies, " *IEEE Trans. Appl. Supercond.*, vol. 31, no. 5, Aug. 2021, Art. no. 2100605.

[12] H. Akamatsu *et al.*, "Progress in the development of frequency-domain multiplexing for the x-ray integral field unit on board the athena mission," *J. Low Temp Phys.*, vol. 199, pp. 737–744, 2020.

[13] D. Vaccaro *et al.*, "Frequency shift algorithm: Application to a frequency-domain multiplexing readout of x-ray transition-edge sensor microcalorimeters," *Rev. Sci. Instrum.*, vol. 92, no. 3, 2021, Art. no. 033103.

[14] M. P. Bruijn *et al.*, "LC filters for FDM readout of the X-IFU TES calorimeter instrument on athena," *J. Low Temp Phys.*, vol. 193, pp. 661–667, 2018.

[15] P. Cor de Vries *et al.*, "Calibration sources and filters of the soft x-ray spectrometer instrument on the hitomi spacecraft," *J. Astron. Telesc. Instrum. Syst.*, vol. 4, no. 1, Oct. 2017, Art. no. 011204.

[16] M. Eckart, C. Kilbourne, and F. Scott Porter, "Instrument calibration report - natural line shapes onboard calibration sources ASTH-SXS-CALDB-LINEFIT, version 0.2," Oct. 2016. Accessed: Mar. 22, 2021. [Online]. Available: https://heasarc.gsfc.nasa.gov/docs/hitomi/calib/caldb_doc/asth_sxs_caldb_linefit_v20161223.pdf, Visited 27/11/2020

[17] P. Peille *et al.*, "XIFU performance requirements document," XIFU-RD-SYS-00278-CNES, Issue 2.2, CNES Tech. Rep. part of the Athena X-IFU I-PRR documentation (10/01/2019).